npj | climate and atmospheric science

www.nature.com/npjclimatsci

ARTICLE OPEN

Check for updates

Overestimation of black carbon light absorption due to mixing state heterogeneity

Linghan Zeng[1,4], Tianyi Tan[1,4], Gang Zhao[1], Zhuofei Du[2], Shuya Hu[1], Dongjie Shang[1] and Min Hu[1,3]✉

Black carbon (BC) aerosols, which arise from incomplete combustion processes, possess the capacity to absorb solar radiation, thereby contributing significantly to the issue of climate warming. However, accurately estimating their radiative effect is challenging, influenced by emissions, sizing, morphology, and mixing state. BC particles undergo aging processes that can alter their physical characteristics and mixing state, consequently affecting their optical properties. In this study, we assessed the mixing state of BC across diverse atmospheric environments. Results demonstrate that mixing state heterogeneity is a ubiquitous phenomenon. In background atmospheres, BC exhibited less homogeneous states compared to those in urban and suburban areas, where heterogeneity was driven by primary emissions. Our study provides direct observational evidence that the heterogeneity of particle-particle mixing can reduce the light absorption enhancement of BC in all atmospheres, with a deviation of up to approximately 24% under background conditions.

npj Climate and Atmospheric Science (2024)7:2 ; https://doi.org/10.1038/s41612-023-00535-8

INTRODUCTION

Black carbon (BC) particles, also known as soot, play an important role in climate change as an effective short-lived climate forcer. BC is mainly formed by the incomplete combustion of biomass, fossil, and biofuels, and the global annual emission of BC was estimated to be 8.54 Tg in 2017[1]. Once emitted, BC particles undergo a series of aging processes, including coagulation, gas-phase condensation, and heterogeneous reactions, consequently altering their optical, physical, and chemical properties. In the recent IPCC AR6, the effective radiative forcing of BC was estimated to be between −0.28 and 0.41 Wm^{-2}, contributing to a temperature rise of 0.1 °C from 1750 to 2019[2]. However, all modeling results are subject to considerable uncertainties, and understanding the aging process of BC is a critical challenge for an accurate and meaningful estimation.

The aging process of BC particles can be simply described as nascent BC (bare BC core or BC thinly coated with co-emitted compounds) gradually grown larger by coating with other non-BC components, which act like a lens focusing more light to the internal BC core, thus enhancing its light absorption[3]. This light absorption enhancement of BC has been confirmed in many laboratory and modeling studies[4–7]. However, ambient measurements have yielded inconsistent results; some studies have observed a significant enhancement in light absorption, while others have reported a much lower enhancement than the results obtained from laboratory and modeling simulations[8–12]. The discrepancies between field studies and laboratory/modeling results have sparked a debate whether climate models have overestimated the climate effects of BC[13,14]. Recent studies, based on simulations of mixing state of BC particles in the ambient atmosphere, proposed that the particle-to-particle heterogeneity in the environment is the main reason for the differences in the enhancement of light absorption between laboratory/modeling results and field observations[15,16]. A field study by Zhai et al.[17] observed both large and minor BC absorption enhancement when the mass ratio between non-BC component and BC core was high and they conclude light absorption enhancement is strongly dependent on the mixing state heterogeneity in coating thickness. However, the impact of BC light absorption due to mixing state has not been fully understood, and it is difficult to incorporate BC mixing state into the global climate model due to its complexity[14]. Yao et al.[18] have shown that a simplified representation of the mixing state of BC (and other aerosol components) may introduce significant errors in aerosol optical properties and further estimate radiative effects. Therefore, a lack of comprehensive understanding of BC heterogeneity is a great challenge in accurately representing the climate impact of BC.

In order to investigate the impact of BC mixing state on the optical properties of BC in the real ambient atmosphere, this study uses an established parameterization scheme to quantify the mixing state heterogeneity of black carbon particles[18–20]. The differences and variations in BC heterogeneity in different ambient air conditions are revealed, and the impact of particle-particle heterogeneity on the light absorption enhancement of BC is discussed.

RESULTS AND DISCUSSION

Overview of the measurement results

The field campaigns at each site lasted approximately 10 days, and the typical levels of air pollutants, temperature, and RH were summarized in Table 1 and Supplementary Fig. 1. As a typical background site, YL has much lower PM_1, SO_2, and NO_x level compared to suburban CP and urban PKUERS. Although the median levels of O_3 were similar at YL and CP, the distribution of O_3 at CP was much wider compared to YL. The O_3 concentration at PKUERS was the lowest among the three sites, possibly due to the combination effect of low solar radiation in winter and titration

[1]State Key Joint Laboratory of Environmental Simulation and Pollution Control, International Joint Research Center for Atmospheric Research (IJRC), College of Environmental Sciences and Engineering, Peking University, 100871 Beijing, China. [2]School of Environmental Science and Safety Engineering, Tianjin University of Technology, 300384 Tianjin, China. [3]School of Environmental Science and Engineering, Nanjing University of Information Science and Technology, 210044 Nanjing, China. [4]These authors contributed equally: Linghan Zeng, Tianyi Tan. ✉email: minhu@pku.edu.cn

Table 1. Summarization of field campaigns at three sites.

Site	Type	Date mm/dd/yyyy	PM_1 μg m^{-3}	BC μg m^{-3}	SO_2 ppbv	NO_x ppbv	O_3 ppbv	Temp °C	RH %
YL	Background	1/21/2015–2/3/2015	5.9	0.4	0.1	1.0	49.4	6.8	51.7
CP	Suburban	5/16/2016–5/26/2016	18.5	2.6	2.9	21.4	54.5	21.8	38.8
PKUERS	Urban	3/23/2015–4/4/2015	59.7	4.2	16.3	68.2	11.5	0.8	27.6

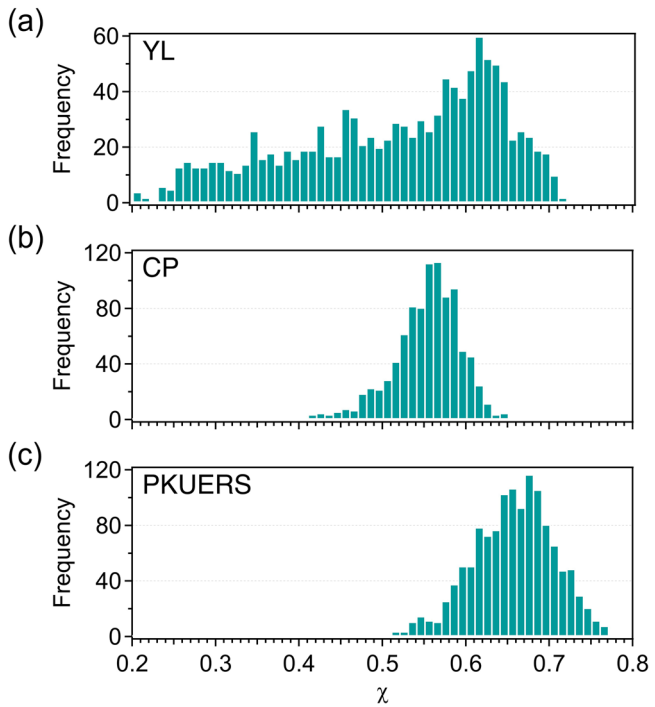

Fig. 1 Frequency histograms of the BC mixing state index. Frequency histograms of the BC mixing state index χ at YL (**a**), CP (**b**), and PKUERS (**c**).

with NO in the urban atmosphere. There were no extreme events or precipitation during the campaigns, ensuring that the measurements taken at YL, CP, and PKUERS were representative of typical background, suburban, and urban conditions, respectively. The time series of BC number and mass concentration is shown in Supplementary Fig. 2, and it exhibited a consistent trend when compared to the time series of PM_1 mass concentration (Fig. 2g, h, i). The mass fraction of BC particles in PM_1 is between ~5 and 10%, with no statistically significant difference observed among the three sites. In the subsequent context, we will focus on the mixing state properties of BC particles.

BC particles are emitted from various sources and undergo distinct atmospheric processes, leading to significant regional differences in their mixing states. In this study, Fig. 1 presents the histogram of the mixing state index χ measured under three different ambient atmospheres, each displaying a distinct distribution. We found that the heterogeneity of BC was a ubiquitous phenomenon as different BC-containing particles have different non-BC to BC ratios. The background station YL exhibited a mode of χ around 0.62, which fell in the middle range among the three sites. Additionally, the distribution ranged from 0.25 to 0.71, suggesting that the BC observed in the high-altitude background site had been influenced by multiple sources. On the contrary, the histograms of χ in urban (PKUERS) and suburban (CP) environments were narrower, indicating that BC sources in both regions had relatively single and steady profiles. The value of χ at PKUERS ranged from 0.5 to 0.75, consistent with the result observed in the winter of 2016 in Beijing[20]. Moreover, the χ distribution at the PKUERS site skewed to the left of the histogram mode at CP, indicating a more homogeneous mixing of BC in the polluted urban atmosphere. This can be attributed to the fact that BC had undergone more complete aging processes under heavily polluted atmospheric conditions, resulting in less variation in coating fraction among different black carbon particles.

In the high-altitude background site YL station, the main source of BC was long-range transport from surrounding regions or vertical upwelling from emissions at lower altitudes[21,22]. The heterogeneities of BC from different air masses behave distinctively. The value of χ was around 0.7 in the early stage (March 23 to 29, 2015) of the field campaign, which subsequently dropped to 0.3 towards the end of the campaign. χ and PM_1 show similar trends during the campaign (Fig. 3a, g). According to back trajectory results, the observed high PM_1 concentration was attributable to air masses transported from South Asia, where biomass burning events occurred frequently over that period, while no dominant source was identified during other times[23]. The high χ observed during the early campaign implies that BC mixed more homogeneously from a single strong source rather than multiple sources. At the later stage of the campaign, χ was lower and became noisier. Regarding the diversity of single particles, D_α shows a slight downward trend, which is similar to χ, being higher at the start and lower at the end. For population diversity parameter, D_γ and χ exhibit a noisy pattern observed in the later stage at YL, while no obvious trends were observed before March 28, 2015. As D_γ was determined by the bulk mass fraction of non-BC to BC mass ratio, the overall ratio of them changed significantly over that time in a clean background atmosphere. We found the mixing state index of BC (χ) under background conditions was dominated by the difference in BC material contribution at the population level, especially at the end of the campaign. To address the issue of noisy data in the later stages of the campaign, primarily arising from the low number/mass concentration of BC-containing particles, potentially resulting in statistically insignificant results, we opted to exclude data points with less than 0.10 μg m^{-3} of BC (equivalent to ~2 μg m^{-3} of PM_1) in the subsequent analysis. Additionally, χ showed a similar trend with F_{thick} in Fig. 2a, g, suggesting F_{thick} may represent the heterogeneity of BC to some extent.

In suburban site CP, it was found that the variation of χ was smaller in comparison to the variations at YL, as shown in Fig. 2b. There was also no significant contrast in χ when the ambient air was clean or moderately polluted, suggesting the pollution level in suburban atmosphere did not have a direct impact on mixing state of BC. However, both D_α and D_γ in Fig. 2e were slightly higher on clean days than under polluted conditions, and they exhibited a clear diurnal variation, also shown in Fig. 3. The value of χ decreased from midnight until 7 am, reaching its minimum value at that time. It then gradually increased till 3 pm, after which it remained relatively high until midnight. The diurnal cycle of χ was the opposite of the mass concentration of thinly coated BC (fresh BC), suggesting that primary emissions dominated the heterogeneity in this region. When primary emissions (e.g., vehicle emissions) were active, the concentration of fresh BC increased dramatically. There was a significant difference in the coating mass fraction between fresh BC particles and background BC,

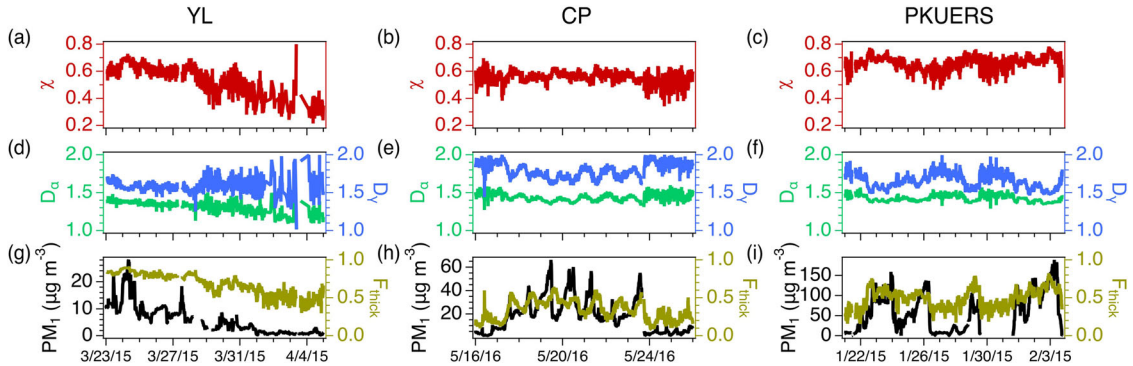

Fig. 2 Time series of BC mixing state parameters during the measurements. Time series of the BC mixing state parameters (χ, $D_α$, $D_γ$, and F_{thick}) and PM_1 mass concentrations at YL (**a**, **d**, **g**), CP (**b**, **e**, **h**), and PKUERS (**c**, **f**, **i**) sites.

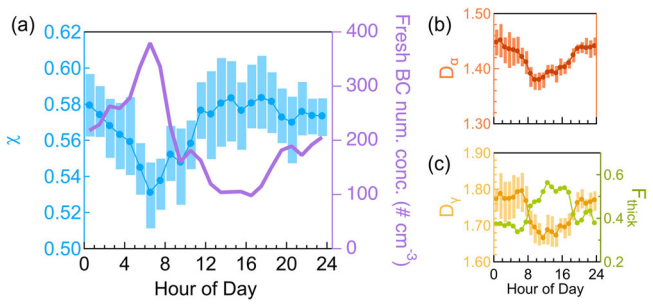

Fig. 3 Diurnal variations of BC mixing state parameters. Diurnal cycles of the BC mixing state index χ and fresh BC number concentration (**a**), the average particle species diversity $D_α$ (**b**), and the bulk population species diversity $D_γ$ and the fraction of thickly coated BC particles (**c**) at CP site. The shading represents the interquartile range of the observation.

which had undergone a high degree of aging. This difference increases the mixing state heterogeneity of BC (lower χ).

$D_α$ and $D_γ$ exhibit similar diurnal trends, with higher levels at night and lower levels during daytime (Fig. 3b, c). However, their patterns were not identical. $D_α$ presents a continuous downward trend from 0 am to 9 am, reaching its lowest point around 10 am and then beginning to rise again. On the other hand, $D_γ$ exhibits a sharp downward trend from 7 am to 12 pm and stays at a lower level until 1 pm. During the night, between evening and morning rush hour, $D_γ$ maintained a relative stable level, suggesting the mass fraction of BC to the overall particle mass did not change much. The population diversity parameter $D_γ$ strongly depends on the fraction of thickly coated BC, which is inferred by a contrary trend of daily variations between $D_γ$ and F_{thick} in Fig. 3c.

The fresh BC (thinly coated) became aged and transformed into thickly coated BC after the morning rush hour, reducing the diversity of BC particles. As the day progressed, the proportion of thickly coated BC continued to increase, reaching its peak in the afternoon. It was likely due to the joint effect of photochemical aging and the weakening of primary emissions. During the evening rush hour (5 pm to 9 pm), accompanied by slower photochemical activities, the proportion of F_{thick} increased, leading to a slight increase in the heterogeneity (lower χ) of BC particles.

During the campaign at urban site PKUERS, three pollution episodes were encountered, and the corresponding χ value increased during the period with high PM. The diurnal cycle of χ at the PKUERS shares some similarities with those at the CP site, with minimum value in the morning rush hour and gradually increasing to the maximum value in the afternoon (Supplementary Fig. 3). But their nighttime behaviors were different: χ remained a lower value at PKU during nighttime, while CP kept in a higher level. A possible explanation for the discrepancy is the seasonal difference. Besides vehicle emissions, biomass burning and coal combustions produced a considerable amount of BC in winter in Beijing, resulting in a less homogeneous mixing state of BC than BC from vehicle emissions in rush hours. In contrast to χ, $D_α$ and $D_γ$ were slightly higher on clean days. The trough of $D_α$ and $D_γ$ coincided with the peak of χ at PKUERS (Fig. 2b, e) and CP (Fig. 3c, i), whereas χ and $D_α$ at the YL site share a similar trend (Fig. 2a, d), suggesting that the dominant factor was not the same in different regions.

In urban and suburban areas, the heterogeneity of BC (χ) not only depends on the air pollution level but also relies on primary BC sources, for example, vehicle emissions and aging processes, and displays a clear diurnal variation. Whereas under background conditions like the YL site, χ strongly depends on the original of air masses; when air masses came from long-range transport of polluted region, χ increased, meaning the BC mixed more homogeneously.

The relationship between BC diversities and F_{thick}

Figure 4 shows the correlation between the BC mixing state index χ with the thickly coated fraction F_{thick}. The χ was strongly correlated with F_{thick} at YL. At the beginning of the campaign (blue points in Fig. 4a), whose particles originated from long-range transport, χ and F_{thick} exhibit an even better correlation. When the air was clean at the end of the measurement, χ and F_{thick} were distributed more scattered but still increased simultaneously. However, χ and F_{thick} have a weak correlation at CP (Fig. 4b). The variation of F_{thick} during the campaign ranged from 0.1 to 0.65, but χ only changed from 0.4 to 0.6. The weak correlation suggests χ did not vary significantly when F_{thick} changed over a large range in environments like CP. At night (dark red and blue in Fig. 4b), F_{thick} was relatively small and had a greater variability, suggesting that CP site were influenced by complex nighttime BC emissions. At PKUERS, χ was moderately correlated with F_{thick}. The distribution of χ is more scattered when F_{thick} is small. Low F_{thick} also matched the period with a low level of air pollution, suggesting BC particles mixed less homogenous. In spite of different degrees of correlation between χ and F_{thick}, χ generally shows an upward trend with F_{thick} in all cases measured in this study.

According to the calculation steps for χ provided in Table 1, BC diversity parameters in terms of both single particles ($D_α$) and population ($D_γ$) codetermine the heterogeneity of BC mixing state χ. Although the χ increases with F_{thick} at three sites (Fig. 4), three regions have totally different relationships between BC diversities ($D_α$ or $D_γ$) with F_{thick} during campaign periods, as shown in Fig. 5. At YL, single particle diversity parameter $D_α$ positively correlated with F_{thick}, but the relationship between population diversity parameter ($D_γ$) was not apparent. However, in urban and suburban atmosphere, both $D_α$ and $D_γ$ show a negative linear

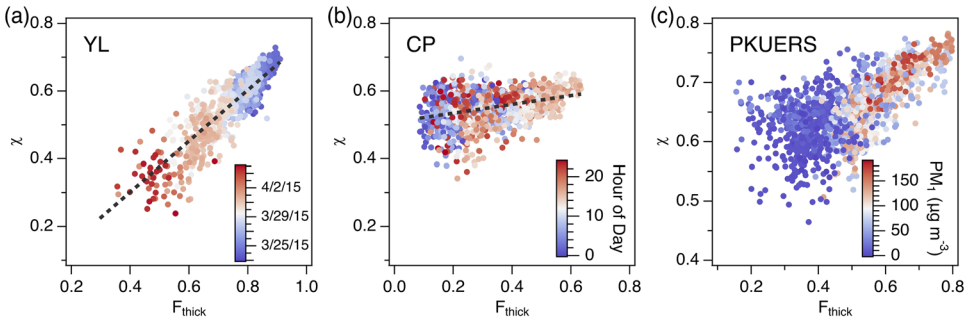

Fig. 4 Relationships between BC mixing state parameters. Scatter plots between the BC mixing state index χ and F_{thick} at YL (**a**) color-coded by date, at CP (**b**) color-coded by hour of day, and at PKUERS (**c**) color-coded by PM_1 mass concentration.

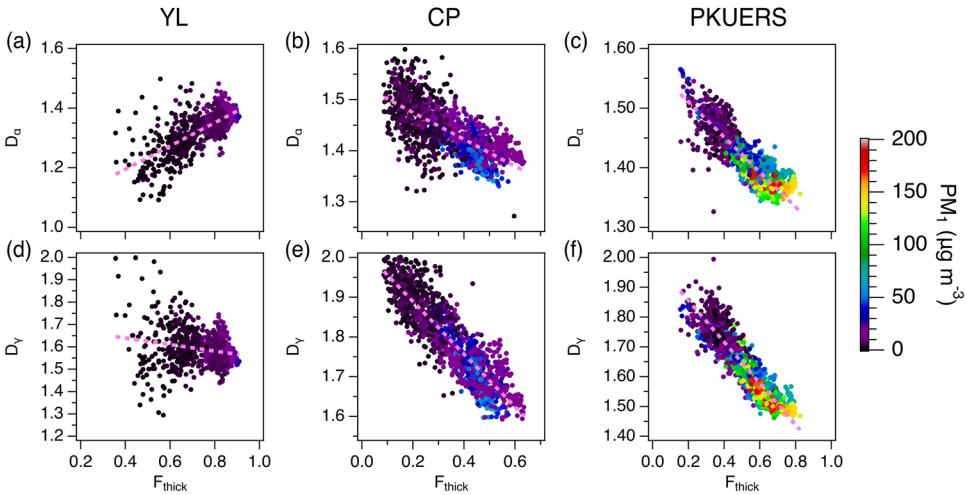

Fig. 5 Relationships between BC diversities and number fraction of thickly-coated BC. Scatter plots between BC diversities (D_α and D_γ) and F_{thick} at YL (**a**, **d**), CP (**b**, **e**), and PKUERS (**c**, **f**), color-coded by PM_1 mass concentration.

relationship with F_{thick}. The discrepancy implies that the dominant factor of BC heterogeneity was different under disparate atmosphere, but all associated with F_{thick}. In addition to F_{thick}, R_{BC} was also a commonly used parameter describing the bulk property of BC mixing state. R_{BC} and F_{thick} exhibit a strong positive correlation at CP and PKUERS but no relationship at YL at all (Supplementary Fig. 4). As both R_{BC} and χ were correlated well with F_{thick} at PKUERS, R_{BC} and χ exhibit a strong correlation (Supplementary Fig. 5), which was also reported in a previous study in winter of 2016 in Beijing. However, R_{BC} and χ distributed very scattered in the summer of 2017 in Beijing, and they concluded R_{BC} cannot used as a metric to predict the variation of χ in summer[20]. Intuitively, both F_{thick} and R_{BC} will increase simultaneously when VOCs or any other gas phase precursors condensed on pre-existing BC-containing particles, making BC particle grow larger, like cases in urban or suburban area. Since BC had many distinct sources and had undergone atmospheric processing at varying extents, R_{BC} and F_{thick} may not be closely related for all ambient conditions, just like the case observed at YL station. As D_γ was directly related to R_{BC}, the relationship between D_γ and F_{thick} was opposite with it between R_{BC} and F_{thick} (Fig. 5e, d, f and Supplementary Fig. 4).

The impact of heterogeneity of BC on light absorption enhancement

Figure 6 shows the time series of the light absorption enhancement (E_{abs}) and the mass ratio of coating material to BC (R_{BC}) during the campaign period at YL. E_{abs} exhibits two distinct stages, corresponding to the two periods discussed in "Methods: Background site (YL)": the period affected by transported pollution and

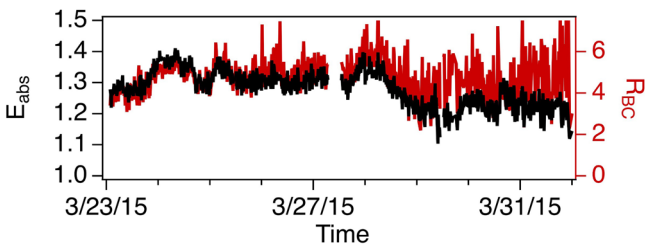

Fig. 6 Times series of BC light absorption enhancement and coating mass ratio. Time series plot of E_{abs} and R_{BC} at YL site.

the period with a clean background. Data after April 1, 2015, were removed as the extremely low BC concentration. E_{abs} was higher before March 28, 2015, fluctuating around 1.3. After that, E_{abs} began to decline and eventually dropped to less than 1.2. However, no consistent pattern was observed in the time series of R_{BC} with E_{abs}, contradicting the power relationship proposed by Chakrabarty and Heinson[12]. E_{abs} and R_{BC} initially exhibited nearly identical trends at the beginning of the campaign. However, after March 28, 2015, they started to diverge, with R_{BC} showing more pronounced fluctuations. This indicates that simply attributing the changes in E_{abs} to the influence of R_{BC} is inadequate and agrees with the findings of Cappa et al.[8] that trends of E_{abs} and R_{BC} do not always exhibit a consistent pattern.

The scatter plot in Fig. 7 illustrates the correlation between E_{abs} and R_{BC} during the campaign period at the YL site. As R_{BC} increases, E_{abs} has an upward tendency but is more scattered. When R_{BC} is less than 1, E_{abs} is mainly around 1.1, indicating that

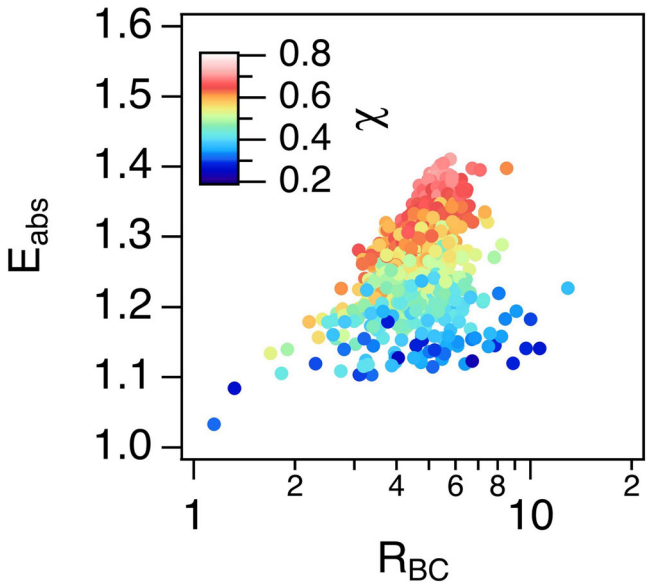

Fig. 7 Relationship between BC light absorption enhancement and coating mass ratio. Scatter plot between E_{abs} and R_{BC} at YL, color-coded with the BC mixing state χ.

the absorption enhancement effect caused by the coating is not significant at low R_{BC} level. When R_{BC} increases to approximately 3, E_{abs} ranges from 1.1 to 1.3, suggesting that there are differences in the absorption enhancement effect under the same R_{BC}. As R_{BC} keeps increasing, the range of E_{abs} variation is even larger. Colors in Fig. 7 reveal that E_{abs} is larger with less heterogeneity of BC (larger χ) at a constant R_{BC} value. Therefore, the light absorption enhancement of BC estimated based only on R_{BC} can be biased without considering the mixing state.

The data measured at YL were binned into intervals of χ value with the increment of 0.2 and fitted with a power function for each bin. As shown in Fig. 8a, power functions can map E_{abs} and R_{BC} well for a small range of χ but are all lower than the case when BC particles were mixed homogeneously (gray line). As the value of χ gets larger, the increasing rate of E_{abs} with respect to R_{BC} also becomes larger. The relative deviation of E_{abs} in Fig. 8b is increasing with respect to R_{BC} and levels off at a large R_{BC} value (logarithmic scale on the bottom axis). When R_{BC} is less than 2, the overestimation of E_{abs} due to BC heterogeneity is less than 10%, while E_{abs} can be overestimated by 24% when R_{BC} increases to ~10. This paper quantifies the influence of mixing state heterogeneity of BC on E_{abs} in the ambient atmosphere and finds that this effect becomes more pronounced with increasing levels of R_{BC}.

For results at CP and PKUERS, the variation of χ was small compared with them at YL, and therefore E_{abs} only varies a small range for a fixed R_{BC} (Fig. 9). R_{BC} at two sites has a similar magnitude but is slightly higher in a more polluted environment: R_{BC} at CP spans from 1 to 5, while it at PKUERS ranges from 2 to 7. The relationship between R_{BC} and E_{abs} is more pronounced and exhibits a power relationship in both regions since χ did not change significantly at either CP or PKUERS. However, E_{abs} of BC at both sites were smaller than in cases where BC was mixed homogeneously with other components. Scatter plots in Fig. 8 show narrower distributions at urban and suburban sites, compared with the result at background site YL. In other words, E_{abs} varies less with the same R_{BC} but still indicates that the light absorption of BC is amplified by coating materials. At PKUERS with larger χ in general, E_{abs} is higher than CP with a similar R_{BC} range. Our observational results provide empirical evidence aligning with previous theoretical studies, showing that the overestimation of black carbon's (BC) light absorption is influenced by mixing state

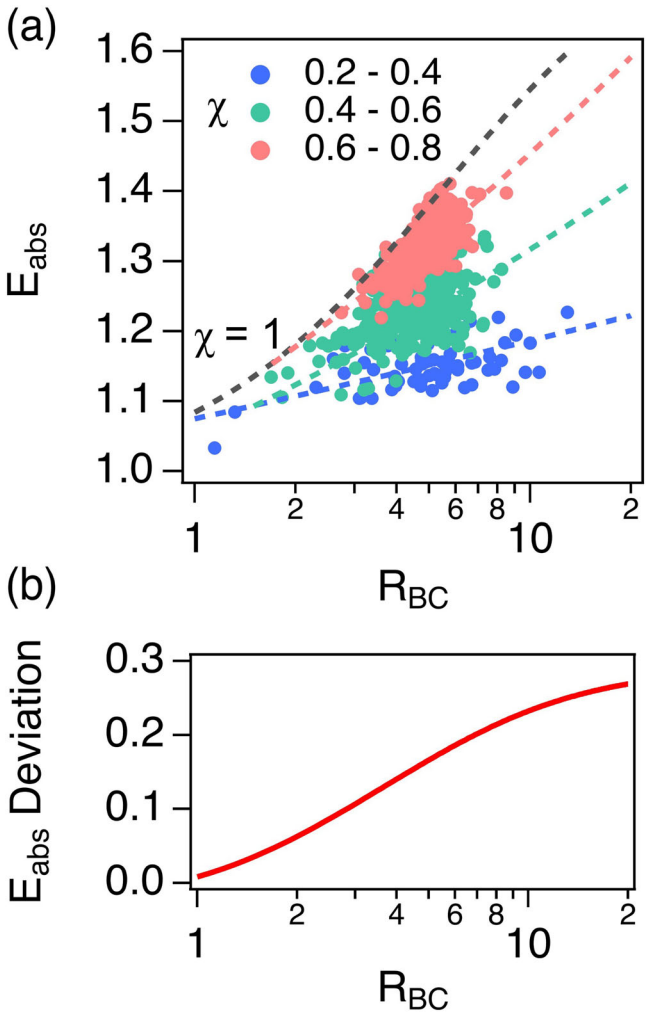

Fig. 8 Deviation of BC light absorption enhancement due to mixing state heterogeneity. a Data in Fig. 6 are binned into intervals of χ value with the increment of 0.2. Solid gray line was the case when all BC particles were mixed homogeneously with $\chi = 1$. Dotted lines were the fitting line of binned data with power laws. **b** The relative deviation of E_{abs} with R_{BC} at YL between two extreme cases, which are homogeneous mixing ($\chi = 1$; gray) and the most heterogeneous case observed at YL ($0.2 < \chi < 0.4$; blue).

heterogeneity. This finding bridges the gap observed between modeled and actual field-measured E_{abs}, resolving a key discrepancy in existing research[8,15,16]. All results indicate that the E_{abs} of BC is overestimated if not considering the heterogeneity of BC. Therefore, the most current models simply assigned a fixed enhancement factor to BC absorption by assuming BC particles were coated uniformly may result in overestimating its absorption and radiative effect.

METHODS

Description of ambient monitoring sites

In this study, extensive field campaigns were carried out at three distinct sites, each representing a specific atmospheric environment: background, suburban, and urban. The geographical positions of these sites are depicted in Supplementary Fig. 6.

Background site (YL). The Yulong Snow Mountain in Lijiang, Yunnan, China, was chosen as the representative background condition for this study. The ambient monitoring station (YL;

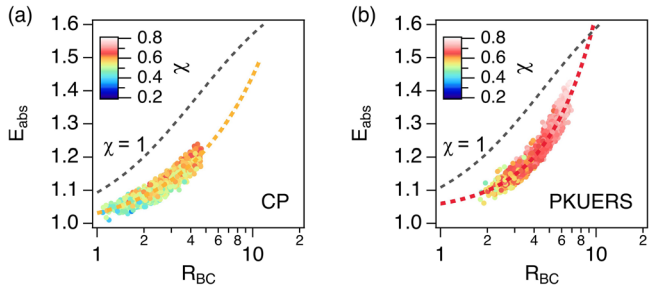

Fig. 9 Less variations in BC light absorption enhancement in suburban and urban environments. Scatter plots between E_{abs} and R_{BC} with CP data (**a**) and PKUERS data (**b**). Data were color-coded with χ. Orange and red lines are data fitted with power functions, and gray lines assume all BC-containing particles were mixed homogeneously at two sites.

27.23 °N, 100.25 °E, 3410 m above sea level) was located in the transitional zone from high to low terrain at the southeastern edge of the Qinghai-Tibet Plateau. Its location connected South Asia and Southeast Asia with the Yungui and Tibet Plateau regions of China, creating a potential pathway for the transport of atmospheric pollutants from South Asia and Southeast Asia into China. The field campaign at the YL background site was conducted from March 23 to April 4, 2015, coinciding with the pre-monsoon season in the region. Previous studies have documented frequent occurrences of biomass-burning events in South Asia and Southeast Asia during this season, and the resulting air masses, influenced by the prevailing southwest monsoon winds, were observed to be transported to the Qinghai-Tibet Plateau[24–27].

Suburban site (CP). The suburban site (CP; 40.24 °N, 116.19 °E) was situated on the roof of the main teaching building (~12 m above ground) at Changping Campus, Peking University, Beijing, China. The campaign at CP took place between May 16 and 25, 2016, during which the average temperature was recorded as 21.8 °C and the relative humidity (RH) was 38.8%. CP, as a typical suburban site, was affected by both natural sources and urban anthropogenic activities[28,29]. The site was located approximately 38 km northwest of central Beijing, with mountainous regions surrounding it on the east, north, and west, covered by extensive green vegetation. Notably, there were no prominent industrial sources in the nearby vicinity.

Urban site (PKUERS). The Peking University Urban Atmospheric Environment Monitoring Station (PKUERS; 39.99 °N, 116.31 °E) was located on the rooftop of an academic building (~20 m above ground) at the main campus of Peking University in the northwest of Beijing, China, was selected as the urban location for this study. The campaign took place from January 21 to February 3, 2015, with an average temperature of 0.8 °C and a RH of 27.6%. The prevailing wind direction during the campaign was from the north, and the wind speeds remained generally low, averaging at 2.2 m s^{-1}. It is worth noting that there were no obvious emission sources in the vicinity of the site, except for Zhongguancun North Street, which was around 200 m east of the site. The traffic restrictions were slightly stricter within the Fifth Ring Road in Beijing, where PKUERS were located. For example, heavy-duty trucks were prohibited from entering the area enclosed by the Fifth Ring Road except between midnight (23:00) and the following day morning (6:00). The PKUERS has been actively monitoring ambient air quality for over a decade, equipped with a range of advanced instruments. The data obtained from this site have provided valuable insights into air pollution in Beijing, as evidenced by previous studies[9,29–31].

Instrumentation

The refractory BC (rBC, or just BC) containing particles were measured by a Differential Mobility Analyzer (DMA, Model 3081, TSI Incorporated, Shoreview, MN, USA)–Single Particle Soot Photometer (SP2, Droplet Measurement Technologies, Longmont, CO, USA) tandem system, and the system setup was illustrated in Supplementary Fig. 7. The detailed description of the DMA-SP2 has been discussed in Zhao et al.[32] and Zhao et al.[19]. Briefly, the DMA scans aerosol size (electrical mobility diameter, D_p) from 12.3 to 749.9 nm in a 5-min cycle, and the SP2 filters out BC-containing particles as BC-containing particles are heated to the point of incandescence when passing through a 1064 nm Nd:YAG laser beam. The induced incandescence signal is nearly proportional to the amount of refractory material (mainly BC). Then, the mass of the BC content (core) can be used to calculate the mass equivalent diameter (D_{MEV} or D_c for simplicity) for each BC-containing particle by assuming a density of 1.8 g cm^{-3}. The SP2 was calibrated using Aquadag, and a correction factor of 0.75 was applied to account for the higher sensitivity of SP2 to Aquadag compared to ambient BC particles[33]. The delay time between the DMA and SP2 was synchronized by the pulse generated by the voltage retrace of the DMA. The correction for the effect of multiple charging was applied using the method proposed by Zhao et al.[32]. BC-containing particles were distinguished as attached-type and coated-type following steps proposed by Dahlkötter et al.[34]. Only coated-type BC particles (>85%) were the subsequent analysis assuming them to be spherical particles. Based on the calibration, the lower detection limit for single BC mass was determined to be 0.32 fg, corresponding to a D_c of 69.7 nm. Therefore, only particles with D_c greater than 69.7 nm were discussed in the subsequent analysis.

Non-refractory chemical compositions of ambient aerosols were measured by a high-resolution time-of-flight aerosol mass spectrometer (HR-ToF-AMS; Aerodyne Research Inc., Billerica, MA, USA). The detailed setup of the instrument and data processing methods were reported in Zheng et al.[27]. The mass concentration of submicron particles (PM_1) was estimated by the sum of non-refractory components and refractory BC, serving as an indicator of the air pollution level.

The mixing ratio of trace gases was measured by gas analyzers (43i for SO_2, 42i for NO_x; 49i for O_3; Thermo Fisher Scientific, Waltham, MA, USA), and meteorology conditions, including temperature, RH, wind speed and wind direction, were measured by sensors manufactured by Met One Instruments Inc., USA.

Description of BC mixing states

Fraction of thickly coated BC (F_{thick}). Different amounts of coating on BC-containing particles can lead to varied responses in the SP2, as indicated by the lag time between the peaks of the scattering signal and the incandescence signal[35,36]. The lag time histogram exhibited two modes for this study, and the split point between the two modes ranged from 1.2 to 1.6 μs. BC-containing particles with a larger lag time were classified as thickly coated BC, whereas particles with a smaller lag time were considered as thinly coated BC. The fraction of thickly coated BC within a specific timeframe is denoted as F_{thick}. Thinly coated BC can be considered fresh BC, whereas thickly coated BC represents aged BC. The classification result for this dataset has been confirmed in our previous study[37]. This parameter does not require any assumption and complex calculation, and can be compared with many studies[38–42].

Mass ratio of non-BC component relative to BC (R_{BC}). The mass ratio of non-BC component relative to BC (R_{BC}) is a widely used bulk property characterizing the BC mixing state[11,43]. We assume that the fraction of each species within the BC coating was proportional to their ambient concentrations, and the densities of each component was obtained in Barnard et al.[44]. The mass of

Table 2. Variables and equations for calculating the BC mixing state index χ[19].

Variables and equations	Descriptions
$p_{i,BC}=\frac{m_{i,BC}}{m_{i,total}}$	Mass portion of BC for each BC-containing particles *i*, where $m_{i,BC}$ and $m_{i,total}$ stand for BC and overall particle mass, respectively.
$m_{BC}=\sum_{i=0}^{N} m_{i,BC}$; $m_{total}=\sum_{i=0}^{N} m_{i,total}$	m_{BC} and m_{total} stand for BC and total mass in the population, respectively.
$p_{BC}=\frac{m_{BC}}{m_{total}}$	Mass portion of BC for all BC-containing particles in the population
$H_i=-[p_{i,BC}\cdot \ln(p_{i,BC})+(1-p_{i,BC})\cdot \ln(1-p_{i,BC})]$	The mixing entropy of each single particle *i*
$H_\alpha=\sum_{i=0}^{N} p_i \cdot H_i$	The average mixing entropy of the population
$H_\gamma=-[p_{BC}\cdot \ln(p_{BC})+(1-p_{i,BC})\cdot \ln(1-p_{i,BC})]$	The population bulk mixing entropy
$D_\alpha=e^{H_\alpha}$	The average particle species diversity parameter (single particle level)
$D_\gamma=e^{H_\gamma}$	The bulk population species diversity parameter (population level)
$\chi=\frac{D_\alpha-1}{D_\gamma-1}$	The dispersion of BC particle mixing state

non-BC components within individual BC-containing particle was estimated with the coating volume, chemical compositions, and the respective density for each species.

Mixing state index of BC (χ). This study employed the BC mixing state index (χ) developed in previous study to quantify the heterogeneity of BC mixing state[18–20]. This method utilized the concept of diversity from ecology[45], and simplified the BC mixing system into a binary system by considering only BC and non-BC components. The BC mixing state index χ can be calculated using the equations listed in Table 2, and it is determined by D_α and D_γ jointly. D_α represents the average particle species diversity parameter, which reflects the diversity of BC mixing states on a single particle level. In contrast, D_γ is a parameter representing the bulk population species diversity. By definition, D_γ is determined by the mass ratio of BC to the total mass, ranging from 1 to 2, while D_α ranges from 1 to D_γ. Consequently, χ varies between 0 to 1. $\chi = 0$ indicates that BC and non-BC components are mixed nearly as external-mixing, while $\chi = 1$ implies that they are mixed homogeneously. Similar to χ, the diversity parameters of BC, either on single particle level (D_α) or population level (D_γ), are lower (close to 1) indicating a higher level of diversity in the mixing of BC.

Light absorption enhancement of BC

The light absorption of both overall BC-containing particles and the corresponding BC cores was calculated using Mie theory at 550 nm[46]. In this study, a perfect core-shell model was assumed, where the BC core and the entire particle were considered spherical, with the core positioned at the center of the particle. The refractive index (RI) of BC core was set to 1.95 – 0.79*i*[47], which is close to the value of engine-emitted BC in visible wavelengths reported by a recent study. The RI of coating material was determined as the volume average of RI of various chemical species reported in the literature[44]. The light absorption coefficient of BC cores and BC-containing particles were obtained by integrating particle number concentration measured by the DMA-SP2 system across the entire size range (e.g., size distributions for each campaign are shown in Supplementary Fig. 8), and the absorption enhancement (E_{abs}) of BC-containing particle was derived by the ratio of light absorption of the overall particle and BC core only.

DATA AVAILABILITY

The data used in this work are archived and can be downloaded from Zenodo (https://doi.org/10.5281/zenodo.8415837; last access: 11/21/2023).

Received: 21 June 2023; Accepted: 27 November 2023;
Published online: 02 January 2024

REFERENCES

1. Xu, H. et al. Updated global black carbon emissions from 1960 to 2017: improvements, trends, and drivers. *Environ. Sci. Technol.* **55**, 7869–7879 (2021).
2. Szopa, S. et al. In *Climate Change 2021: The Physical Science Basis.* Contribution of Working Group I to the Sixth Assessment Report of the Intergovernmental Panel on Climate Change (eds Masson-Delmotte, V. et al.) (IPCC, 2021).
3. Lack, D. A. & Cappa, C. D. Impact of brown and clear carbon on light absorption enhancement, single scatter albedo and absorption wavelength dependence of black carbon. *Atmos. Chem. Phys.* **10**, 4207–4220 (2010).
4. Fuller, K. A., Malm, W. C. & Kreidenweis, S. M. Effects of mixing on extinction by carbonaceous particles. *J. Geophys. Res. Atmos.* **104**, 15941–15954 (1999).
5. Schnaiter, M. et al. Absorption amplification of black carbon internally mixed with secondary organic aerosol. *J. Geophys. Res. Atmos*. **110**, D19204 (2005).
6. Khalizov, A. F., Xue, H., Wang, L., Zheng, J. & Zhang, R. Enhanced light absorption and scattering by carbon soot aerosol internally mixed with sulfuric acid. *J. Phys. Chem. A* **113**, 1066–1074 (2009).
7. Zhang, Y. et al. Evidence of major secondary organic aerosol contribution to lensing effect black carbon absorption enhancement. *NPJ Clim. Atmos. Sci.* **1**, 47 (2018).
8. Cappa, C. D. et al. Radiative absorption enhancements due to the mixing state of atmospheric black carbon. *Science* **337**, 1078–1081 (2012).
9. Peng, J. et al. Markedly enhanced absorption and direct radiative forcing of black carbon under polluted urban environments. *Proc. Natl Acad. Sci. USA* **113**, 4266–4271 (2016).
10. Wu, Y. et al. Light absorption enhancement of black carbon aerosol constrained by particle morphology. *Environ. Sci. Technol.* **52**, 6912–6919 (2018).
11. Liu, D. et al. Black-carbon absorption enhancement in the atmosphere determined by particle mixing state. *Nat. Geosci.* **10**, 184–188 (2017).
12. Chakrabarty, R. K. & Heinson, W. R. Scaling laws for light absorption enhancement due to nonrefractory coating of atmospheric black carbon aerosol. *Phys. Rev. Lett.* **121**, 218701 (2018).
13. Brown, H. et al. Biomass burning aerosols in most climate models are too absorbing. *Nat. Commun.* **12**, 277 (2021).
14. Wang, J. et al. Unified theoretical framework for black carbon mixing state allows greater accuracy of climate effect estimation. *Nat. Commun.* **14**, 2703 (2023).
15. Fierce, L. et al. Radiative absorption enhancements by black carbon controlled by particle-to-particle heterogeneity in composition. *Proc. Natl Acad. Sci. USA* **117**, 5196–5203 (2020).
16. Fierce, L., Bond, T. C., Bauer, S. E., Mena, F. & Riemer, N. Black carbon absorption at the global scale is affected by particle-scale diversity in composition. *Nat. Commun.* **7**, 12361 (2016).
17. Zhai, J. et al. Absorption enhancement of black carbon aerosols constrained by mixing-state heterogeneity. *Environ. Sci. Technol.* **56**, 1586–1593 (2022).
18. Yao, Y., Curtis, J. H., Ching, J., Zheng, Z. & Riemer, N. Quantifying the effects of mixing state on aerosol optical properties. *Atmos. Chem. Phys.* **22**, 9265–9282 (2022).
19. Zhao, G., Tan, T., Zhu, Y., Hu, M. & Zhao, C. Method to quantify black carbon aerosol light absorption enhancement with a mixing state index. *Atmos. Chem. Phys.* **21**, 18055–18063 (2021).

20. Yu, C. et al. Characterising mass-resolved mixing state of black carbon in Beijing using a morphology-independent measurement method. *Atmos. Chem. Phys.* **20**, 3645–3661 (2020).
21. Wang, M. et al. Black carbon profiles from tethered balloon flights over the southeastern Tibetan Plateau. *Chin. Sci. Bull.* **64**, 2949–2958 (2019).
22. Niu, H., Shi, X., Gang, L., JunHua, Y. & ShiJin, W. Characteristics of total suspended particulates in the atmosphere of Yulong Snow Mountain, southwestern China. *Sci. Cold Arid Reg.* **10**, 207–218 (2018).
23. Tan, T. et al. Measurement report: strong light absorption induced by aged biomass burning black carbon over the southeastern Tibetan Plateau in pre-monsoon season. *Atmos. Chem. Phys.* **21**, 8499–8510 (2021).
24. Marinoni, A. et al. Aerosol mass and black carbon concentrations, a two year record at NCO-P (5079 m, Southern Himalayas). *Atmos. Chem. Phys.* **10**, 8551–8562 (2010).
25. Zhao, Z. et al. Aerosol particles at a high-altitude site on the Southeast Tibetan Plateau, China: implications for pollution transport from South Asia. *J. Geophys. Res. Atmos.* **118**, 11,360–11,375 (2013).
26. Pani, S. K. et al. Black carbon over an urban atmosphere in northern peninsular Southeast Asia: characteristics, source apportionment, and associated health risks. *Environ. Pollut.* **259**, 113871 (2020).
27. Zheng, J. et al. Influence of biomass burning from South Asia at a high-altitude mountain receptor site in China. *Atmos. Chem. Phys.* **17**, 6853–6864 (2017).
28. Zhang, Y. et al. Source apportionment of $PM_{2.5}$ pollution in the central six districts of Beijing, China. *J. Clean. Prod.* **174**, 661–669 (2018).
29. Tang, R. et al. Primary and secondary organic aerosols in summer 2016 in Beijing. *Atmos. Chem. Phys.* **18**, 4055–4068 (2018).
30. Guo, S. et al. Elucidating severe urban haze formation in China. *Proc. Natl Acad. Sci. USA* **111**, 17373–17378 (2014).
31. Zamora, M. L. et al. Wintertime aerosol properties in Beijing. *Atmos. Chem. Phys.* **19**, 14329–14338 (2019).
32. Zhao, G., Zhao, W. & Zhao, C. Method to measure the size-resolved real part of aerosol refractive index using differential mobility analyzer in tandem with single-particle soot photometer. *Atmos. Meas. Tech.* **12**, 3541–3550 (2019).
33. Laborde, M. et al. Sensitivity of the Single Particle Soot Photometer to different black carbon types. *Atmos. Meas. Tech.* **5**, 1031–1043 (2012).
34. Dahlkötter, F. et al. The Pagami Creek smoke plume after long-range transport to the upper troposphere over Europe—aerosol properties and black carbon mixing state. *Atmos. Chem. Phys.* **14**, 6111–6137 (2014).
35. Shiraiwa, M. et al. Evolution of mixing state of black carbon in polluted air from Tokyo. *Geophys. Res. Lett.* **34**, L16803 (2007).
36. Moteki, N. & Kondo, Y. Effects of mixing state on black carbon measurements by laser-induced incandescence. *Aerosol Sci. Technol.* **41**, 398–417 (2007).
37. Zhao, G. et al. Mixing state of black carbon at different atmospheres in north and southwest China. *Atmos. Chem. Phys.* **22**, 10861–10873 (2022).
38. Schwarz, J. P. et al. Single-particle measurements of midlatitude black carbon and light-scattering aerosols from the boundary layer to the lower stratosphere. *J. Geophys. Res. Atmos.* **111**, D16207 (2006).
39. Saha, P. K., Khlystov, A. & Grieshop, A. P. Downwind evolution of the volatility and mixing state of near-road aerosols near a US interstate highway. *Atmos. Chem. Phys.* **18**, 2139–2154 (2018).
40. Metcalf, A. R. et al. Black carbon aerosol over the Los Angeles Basin during CalNex. *J. Geophys. Res. Atmos.* **117**, D00V13 (2012).
41. Pan, X. et al. Emission characteristics of refractory black carbon aerosols from fresh biomass burning: a perspective from laboratory experiments. *Atmos. Chem. Phys.* **17**, 13001–13016 (2017).
42. Ko, J., Krasowsky, T. & Ban-Weiss, G. Measurements to determine the mixing state of black carbon emitted from the 2017–2018 California wildfires and urban Los Angeles. *Atmos. Chem. Phys.* **20**, 15635–15664 (2020).
43. Wang, J. et al. Characteristics and sources of ambient refractory black carbon aerosols: insights from soot particle aerosol mass spectrometer. *Atmos. Environ.* **185**, 147–152 (2018).
44. Barnard, J. C., Fast, J. D., Paredes-Miranda, G., Arnott, W. P. & Laskin, A. Technical Note: Evaluation of the WRF-Chem "aerosol chemical to aerosol optical properties" module using data from the MILAGRO campaign. *Atmos. Chem. Phys.* **10**, 7325–7340 (2010).
45. Riemer, N. & West, M. Quantifying aerosol mixing state with entropy and diversity measures. *Atmos. Chem. Phys.* **13**, 11423–11439 (2013).
46. Bohren, C. F. & Huffman, D. R. *Absorption and Scattering of Light by Small Particles* (Wiley, 1983).
47. Moteki, N., Kondo, Y. & Nakamura, S.-I. Method to measure refractive indices of small nonspherical particles: application to black carbon particles. *J. Aerosol Sci.* **41**, 513–521 (2010).

ACKNOWLEDGEMENTS

This study was financially supported by the National Key Research and Development Program of China (2022YFC3701004, task4).

AUTHOR CONTRIBUTIONS

L.Z. and T.T. analyzed the data and wrote the paper. T.T., G.Z. and M.H. designed the project. Z.D., S.H. and D.S. made measurements and analyzed the data. All authors reviewed and provided comments for the paper.

COMPETING INTERESTS

The authors declare no competing interests.

ADDITIONAL INFORMATION

Supplementary information The online version contains supplementary material available at https://doi.org/10.1038/s41612-023-00535-8.

Correspondence and requests for materials should be addressed to Min Hu.

Reprints and permission information is available at http://www.nature.com/reprints

Publisher's note Springer Nature remains neutral with regard to jurisdictional claims in published maps and institutional affiliations.